Journal of Materials Chemistry A

Accepted Manuscript

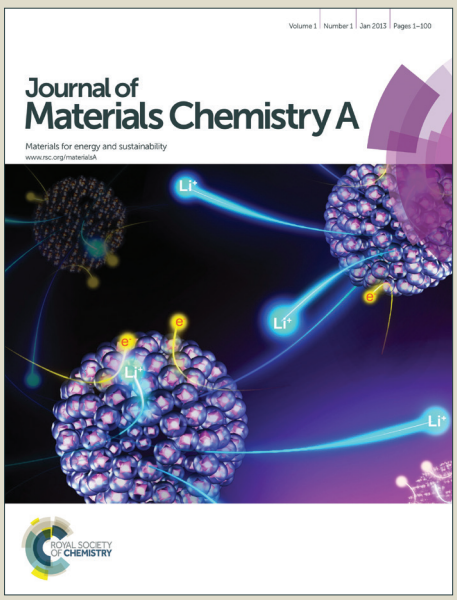

ROYAL SOCIETY OF CHEMISTRY

www.rsc.org/materialsA

Journal Name

RSCPublishing

ARTICLE

Self-assembled photoactive heterojunction phase gradient

Cite this: DOI: 10.1039/x0xx00000x

G. Merle,[a] D. C. Bassett,[a] J. A. Finch,[b] G. Demopoulos,[b] and J. E. Barralet[a, c]

Received 00th January 2012,
Accepted 00th January 2012

DOI: 10.1039/x0xx00000x

www.rsc.org/

The high photocatalytic activity of anatase is markedly enhanced by the presence of a rutile interface. Such phase heterojunctions have previously been formed by sintering admixtures, which results in biphasic particles or agglomerated powders. Current efforts to orientate these heterojunctions relative to the incident light and electrodes to optimize and further improve photoactivity have focussed on sputter coating, dip coating and doctor blading. These techniques offer two ways by which photoactivity may be increased; firstly by maximizing the area of the heterojunction relative to the volume of the two phases and secondly by optimizing spatial ordering of the phases, charge carrier flow direction and path length. Here we report a one step room temperature self-assembly technique which reproducibly creates microstructurally phase graduated photoanodes consisting of a base layer of rutile nanorods and increasing concentrations of anatase in subsequent layers. A large increase in current density and OCP was observed (0.4 to 0.75 mA/cm^2) that coincided with the appearance of anatase in the coating *i.e.* the initial formation of a heterojunction, and longer deposition times were concomitant with increasing current density to a maximum of 1.1 mA/cm^2 The resulting nanostructured electrodes were evaluated in non-optimised N3-dye-sensitized solar cells (DSSCs) where they demonstrated 188% higher short current density than P25 controls.

Introduction

Dye sensitized solar cells (DSSCs) have emerged as cost effective alternatives to photovoltaic devices since their invention by Grätzel *et al*.[1]. Typically, commercial DSSCs (*e.g.* by G24 Innovations, 3GSolar, Solarprint, Sony, Samsung, TiSol, Sharp, *etc*.) are composed of a TiO_2 photoanode, a photosensitising dye, an electrolyte based on an I^-/I^-_3 couple and a Pt counter-electrode. The TiO_2 photoelectrode transports photogenerated electrons from the dye to the back of the electrode and supplies the photogenerated hole to the electrolyte. Anatase, the most photo-catalytically active TiO_2 phase with low rates of charge recombination[2] and high adsorptive affinity for organic compounds[3, 4], has been used extensively for photoelectrodes, and it has been established that the incorporation of a small amount of rutile considerably enhances the photocatalytic properties of the electrode by the creation of a biphasic heterojunction[4-6]. These junctions are present in Degussa P25[4, 7, 8], one of the most widely studied TiO_2 photocatalysts, which consists of anatase (85%) and rutile (15%) in the form of biphasic particles some 25 nm in diameter[8]. It has been shown that the separation of photogenerated holes and electrons occurring at heterojunctions manifests due to a difference in band gap between the phases giving rise to enhanced photocatalytic activity[6, 9]. At these heterojunctions, strongly coupled photo-excited electrons and holes can preferentially move to the rutile or anatase phase respectively, thereby further limiting electron-hole recombination[5, 10]. There are a variety of methods to form biphasic titania powders [8, 11] but in all of these syntheses the organisation of heterojunctions is somewhat random and only size and phase fraction can be modified.

The use of a passivating rutile layer beneath an upper layer of photoactive anatase has also been found to increase the conversion efficiency by minimising the back transfer of electrons to the redox ion in the electrolyte and their subsequent recombination[12]. Currently there are only a few studies reporting the use of orientated heterojunctions, in which the two phases are spatially located in the same regions of the device allowing for efficient charge collection; these structures are achieved *via* sputtering[13], facing target sputtering[14], dip-coating[15, 16] and layer by layer deposition of anatase nanoparticles on the surface of 1D rutile nanorods[17]. When the two phases are in close contact and spatially ordered, the photoexcited electrons' and holes' flow path and distance can be optimized resulting in higher solar conversion efficiencies compared to DSSCs prepared without a passivating rutile layer[12].

We discovered a concentration dependent effect of phytic acid (PA) concentration promoting the aqueous formation of nanocrystalline (2-3nm) anatase as opposed to the more stable rutile, however its photoactivity was negligible prior to heat treatment. Calcination determined the anatase phase to be stable up to 800˚C and that optimal activity was imparted after heating at 600˚C. This was unexpected because the phase conversion temperature of anatase to rutile is reported to be 600˚C [18, 19] and usually nanosized materials have lower thermal stability than their microcrystalline counterparts[19]. Here we applied this new room temperature synthesis to self-assemble organised rutile-anatase heterojunctions

from biphasic mixtures of titania *via* phase mobility selective electrodeposition. This simple method to create a continuous 2D heterojunction generated a photocurrent in an N3-DSSC nearly twice as high as that achieved in an equivalent P25 electrode in which the heterojunctions were randomly oriented.

Results and discussion

Decomposition of $TiOCl_2$ in the absence of PA resulted in the formation of phase pure rutile, however the addition of PA at Ti: PO_4 ratios of 146:1 and 44:1 resulted in the formation of biphasic mixtures with increasing proportions of anatase with increasing proportions of PO_4, until a ratio of 29:1 after which phase pure anatase was obtained (**Figure 1**).

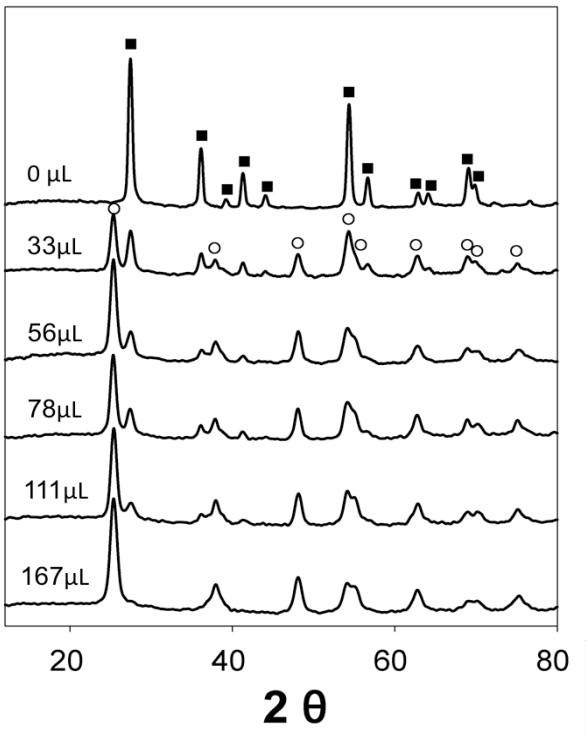

Figure 1: Effect of PA addition on the phase composition of TiO_2 formed in the presence of an ultrasonic field and subsequent heat treatment at 600°C. ■ – Rutile, ○ – Anatase.

PA reduced the crystallite size of both rutile and anatase, but at high concentrations surface area decreased, a change not reflected in crystallite size (**Table 1)**. Surface phosphate has previously been reported to minimise anatase growth during calcination[20]. Despite a Ti:P ratio of 44:1 in the reaction mixture, XRF measurements indicated the amount of phosphorous present in PA modified samples calcined at 600 ºC to be 1.5 wt%, giving a Ti:P molar ratio of 20:1, which is less than the saturation concentration of phosphate adsorption on titania [20]. It seems probable that the changes in phase and area were a result of complexation of the titanium ions formed during hydrolysis which would have reduced the degree of supersaturation thereby promoting the anatase phase[21]. Further support for this theory came from the experimental observation that if the two solutions were rapidly mixed, rutile was formed immediately yet if the solutions were added slowly, no precipitate formed initially and anatase was precipitated slowly over the following 24 hours.

Table 1. Comparison of physicochemical properties of TiO_2-PO_4 samples

Ti: P	% Anatase[(a)]	Specific Surface area [$m^2 g^{-1}$]	Band gap energy [(b)][eV]	Isoelectric point
0	0	14.1	3.04	1.72
146:1	54	53.9	3.01	1.88
88:1	76	88.1	2.99	1.99
63:1	73	99.6	2.98	2.19
44:1	84	75.2	2.97	2.22
29:1	100	69.0	2.95	2.58
P25	80	52.4	3.21	6.70

a) Estimated from XRD data
b) Estimated from diffuse reflectance spectra measurements

A high surface area photoanode is advantageous for DSSCs since a larger amount of dye can be adsorbed and hence an increase in photo-conversion is expected. We observed a near linear ($R^2 = 0.91$) increase in photocurrent with surface area (**Figure 2**) for biphasic mixtures and a subsequent reduction from the maximum value.

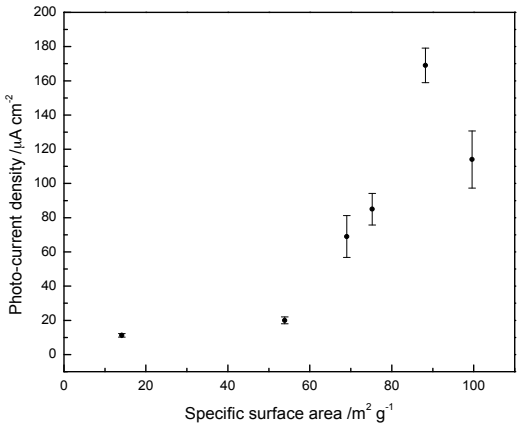

Figure 2: Mean of photocurrent density (N=3) vs. surface area for samples treated with different amounts of PA and after heat treatment at 600°C for 1 h. Photocurrent was acquired at OCP (vs. Ag/AgCl electrode).

Other studies of more simple single phase systems have determined that the electron diffusion coefficient increases with particle size and recombination time decreases with specific surface area [22]**.** One can speculate that the ideal phase ratio for mixed anatase and rutile systems would depend on geometry and dimension, since particle number per unit mass is inversely proportional to the cube of particle dimension. Relative particle numbers affect heterojunction area, which in turn affects recombination rate. It is reasonable to suppose that at this high surface area and hence small particle size, recombination rate increased relative to electron transfer. The presence of rutile in mixed titania phases results in an increased photogenerated current by preventing carrier recombination due to the difference in band gap between anatase and rutile and by a higher light harvesting

efficiency favoured by the presence of the rutile phase[23]. Only a small amount of visible-light absorption was detected in PA modified titania, the main absorption edge of P25 was estimated to be about 386 nm (3.21 eV) whereas the TiO_2-PO_4 showed a shoulder peak at a wavelength of around 421-408 nm (3.04-2.95 eV) (**Table 1 and Figure S1**). A similar effect due to non-metal doping has been shown previously[24] with carbon[25], phosphate[26], and nitrogen[27] doped titania films in which it has been shown that the anions increased visible absorption (λ 400 nm) of the TiO_2 higher than that of pristine TiO_2 by either substituting the oxygen in the titania lattice or by placing the element at interstitial sites[28], leading to higher photoactivity under solar light.

Theoretically the ideal anatase-rutile configuration in a DSSC would maximise the contact area between the two phases to minimise recombination. Additionally, because of the band gap difference, holes flow preferentially to the anatase phase that should be in contact with the dye to oxidise the iodine ion in the electrolyte. In contrast, the rutile should be in contact with the electrode to allow electron flow to do electrical work. Furthermore, because rutile has a higher refractive index than anatase (2.609 *vs* 2.488), it is a stronger scatterer and promotes photon trapping by internal reflection and hence further improves overall photo-efficiency.

Previous attempts to produce this architecture have all been two-step processes [15, 29] that are expensive and complex and the region of heterojunction is limited to the interface between the two coatings. Electrodeposition is an elegant method for creating layered coatings from biphasic mixtures[30], but to date this process has not been applied to the optimisation of titania microstructures for DSSC. A possible reason is that anatase typically has a higher magnitude of zeta potential than rutile in aqueous solutions[31] and therefore has a higher electrophoretic mobility as predicted by Henry's law which creates the opposite conditions to those necessary for an anatase coating on rutile. Recently, only completely homogenous biphasic anatase-rutile coatings for photodegradation were achieved by selecting aqueous dispersants that rendered the zeta potentials of anatase and rutile equal allowing simultaneous deposition[32].

A problem with aqueous solvents for electrodeposition of titania is that water splitting into hydrogen and oxygen occurs at potentials as low as 1.64 V at pH 7. This creates pinholes in the coating and contaminates the coating with the ions used to increase conductivity. By adapting the approach using a mixture of acetyl acetone and iodine[30], we obtained a well-dispersed stable suspension and unexpectedly the rutile in this electrolyte possessed a higher magnitude of zeta potential (52.3mV) than anatase (39.9 mV), compared with pH 7 buffer (-46.5 and -51 mV and thereby exhibited a greater electrophoretic mobility (0.94 vs. 0.71 mm cm Vs^{-1}) than anatase. This enabled heterogeneously deposition of at first a rutile rich layer and subsequently a concentration gradient of an increasing proportions of anatase. (**Table 2**)

Table 2: Comparison of the mass and phase composition of 88:1 T_i:PA at different stages of electrophoretic deposition.

EPD time [s]	Mass deposition [mg]	Anatase/Rutile ratio[(a)]
60	0.5±0.2	0.26
120	1.8±0.4	0.40
180	4.3±0.3	0.55
250	6.8±0.2	0.60

[(a)] Estimated from XRD data

We observed that upon application of a cathodic potential of 5.0V vs. Ag/AgCl a deposition time of more than 250 seconds resulted in poor adhesion of the film. Phase composition and cross-sections of the films after increasing deposition times were examined with XRD and SEM respectively. As the film grew over the time, XRD of the films revealed that first rutile rich material was deposited followed by an increasing proportion of anatase (**Figure 3**).

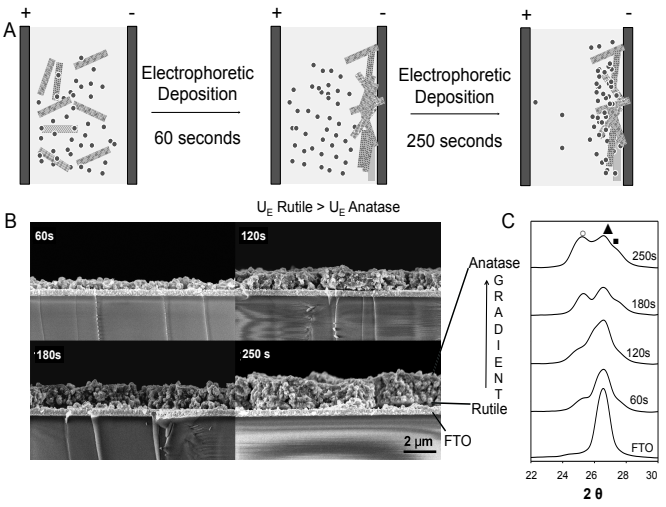

Figure 3: A) Electrophoretic deposition process, B) SEM images of the cross section of 88:1 TiO_2-PO_4 films at 60, 120, 180 and 250 seconds of electrophoretic deposition and after heat treatment at 600°C and C) XRD patterns illustrating effect of electrophoretic deposition time on the phase composition of TiO_2 layer on the electrode following heat treatment at 600°C. ○ – Anatase, ■ – Rutile, ▲- FTO. Arrows to SEM images to guide the eye as to where the diffraction patterns were obtained.

The surface of the films after 60 sec deposition, consisted of a uniform film of particles (>100 nm), and at later times much smaller (10-20 nm) particles which were present both as discrete particles and aggregated "nodules" of larger particles coated with a smaller phase (**Figure 4**).

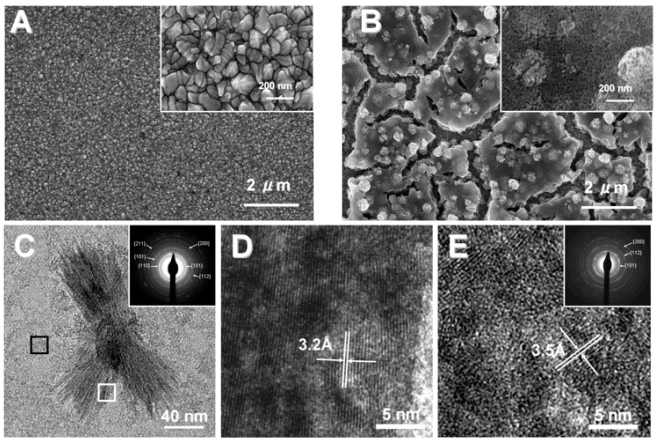

Figure 4: SEM images of the TiO_2-PO_4 films at 60 (A) and 250 seconds (B) of electrophoretic deposition and after heat treatment at 600°C; Transmission electron micrographs and associated electron diffraction patterns of TiO_2-PO_4 following 250 seconds electrophoretic deposition. **C:** Large acicular crystals of rutile and much smaller anatase nanoparticles were found. Electron diffraction

confirmed a mixed phase of rutile and anatase. **D**: High magnification of white square in C, lattice measurements confirmed the rutile phase. **E**: High magnification of black square in C, lattice measurements confirmed the anatase phase and a particle size of approximately 6-10 nm.

To further examine particles in detail, titania deposited after 250 sec was physically removed from the substrate and examined using TEM. This revealed that after heat treatment the film was composed of rutile nanorods of more than 100 nm length arranged in rosettes and small discrete spherical anatase nanoparticles 10 nm in diameter. Electron diffraction and lattice space measurements further confirmed rutile nanorods and anatase nanoparticles (**Figure 4**). We attempted to apply the EPD process using a mixture of commercial anatase nanopowder and rutile prepared with phytic acid. We were unable to detect the development of a heterojunction by XRD and the photocurrent was similarly low as P25. It appears that the lack of agglomeration and the fine particle size are a key feature phytic acid synthesis, necessary for the biphasic gradient during deposition.

Upon photon irradiation, an increasing negative shift in the open circuit potential (OCP) was observed (**Figure 5**) reflecting an increase in the steady state concentration of electrons in the conduction band of the semi-conductor. There was also a similar correlation observed between the photocurrent density at OCP vs. Ag/AgCl and the deposition time (**Figure 5**).

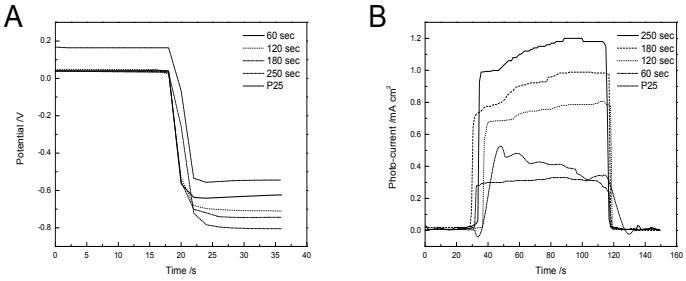

Figure 5: **A**: Open circuit potential characteristics curves measured upon illumination and in the dark of the as-prepared photo-anodes at 60, 120, 180 and 250 seconds with 88:1 TiO_2-PO_4 and at 250 seconds with P25 samples. **B**: Current density−time characteristics curves measured upon illumination and in the dark of the as-prepared photo-anodes at 60, 120, 180 and 250 seconds with 88:1 TiO_2-PO_4 and at 250 seconds with P25 samples.

A large increase in current density and OCP was observed as the deposition time increased from 60 to 120 seconds followed by a gradual increase until 250 seconds (**Figure 5**). After a deposition time of 120 seconds, anatase was gradually electrodeposited on the rutile. This large increase in current density (0.4 to 0.75 mA/cm^2) coincided with the appearance of anatase (**Figure 3**), *i.e.* the initial formation of heterojunctions, and the subsequent slight increase in current density observed in coatings formed at longer deposition times is concomitant with the increased concentration of anatase in subsequent layers, essentially reducing the proportion of heterojuctions. We applied the EPD process using phase pure anatase and high surface area nanopowder prepared with phytic acid to produce a photoanode. The photogenerated current was lower compared to our lower surface area heterophase anodes (**Figure S3**). SSA appears therefore to be not an exclusive parameter in photoconversion. Our mixed phase EDP anatase-rutile configuration gaveho rise to a rutile-rich layer with an overlying gradient of anatase that resulted in a smooth electron and hole flow and by a higher light harvesting efficiency favoured by the presence of the rutile phase[23]. The recombination processes was studied with open-circuit voltage decay[33]. Electrons were recorded upon and after illumination on the unsensitised photoelectrodes. After interruption of illumination, a slow increase in photovoltage is observed for the heterojucntion photoelectrode whereas the increase in photovoltage is quasi immediate for P25 photoelectrode. After illumination and at open circuit, the excess of electrons only can be removed by recombination and the electron lifetime is directly related to the rapidity of the decay of the photovoltage by the expression:

$$\tau_n = -\frac{\kappa b.T}{e}\left(\frac{d\,V_{OC}}{dt}\right)^{-1} \qquad \text{Equation (1)}$$

where τ_n, $\kappa b.T$, e and V_{OC} are electron lifetime, thermal energy coefficient, positive elementary and open-circuit voltage charge respectively. Our mixed phase with the rutile blocking layer and the anatase gradient drastically decreased the electron recombination compared to the P25 (**Figure S4**).

Following these experiments the photo-anodes prepared with a deposition time of 250 seconds were chosen as lead candidate samples for DSSC evaluation.

The current density-voltage characteristics for DSSCs prepared with biphasic titania and P25 photo anodes (**Figure 5**) and the corresponding cell parameters are listed in **Figure S5** The overall photovoltaic conversion efficiency (η) was calculated by:

$$\eta = \left(J_{sc} \times V_{oc} \times FF\right) \div P_{In} \qquad \text{Equation (2)}$$

where J_{sc}, V_{oc} and FF are short current density, open-circuit voltage and fill factor respectively. P_{In} refers to the incident light intensity used (100 mW cm^{-2})[34]. There was only a very slight difference in V_{oc} between biphasic titania and P25 based DSSCs. However, the TiO_2-PO_4 photoanodes exhibited a much higher J_{sc} of 14 mA cm^{-2} compared to 8 mA cm^{-2} for P25. The structure of the photo-anode comprising of rutile nanorods and smaller anatase nanoparticles resulted in a high surface area for dye chemisorption as well as enhanced light scattering. Additionally, charge transfer was enhanced due to the presence of abundant heterojunctions between the two phases, which stabilize electron–hole pair separation by locating the electrons and holes in the different crystalline phases. A key feature of our DSSC is the presence of rutile in intimate contact with the FTO layer that provides a direct route for electrons to the back contact of the electrode, reduces the rate of recombination and thus increases the charge collection efficiency compared to the nanoparticles. The moderate increase in performance is mainly due to a slight decrease in FF. Therefore a further improvement in FF would enhance DSSC efficiency far exceeding that of P25. The internal series resistance including the resistances of the glass substrate, interface TiO_2/glass, counter electrode and electrolyte of the DSC are what mainly influences the fill factor. The enhancement in FF could be achieved by minimising this series resistance[35, 36] with respect to a) the ion transport processes in the electrolyte (transport rate and transport distance), b) the charge-transfer processes occurring at the Pt counter electrodes to accelerate the reduction rate of I_3^- to I^- and c) the sheet resistance of the FTO substrates. FF can be affected by the concentration of I_2 in electrolyte, i.e. a increase of I_3^- concentration will decrease the resistance related to diffusion of I_3^- thus raise the FF value[35]. The charge transfer resistance in the counter electrode (CE) can as well directly affect the FF. Rhee and al.,[37] suggested that the increase of

the layer thickness at the CE decreased the charger transfer resistance due to the enhancement of the electron transfer process at CE/ electrolyte interface.

Experimental

Materials

Titanium Dioxide nanopowder (Aeroxide® P25 TiO_2, Ø ~ 20 nm) was supplied by Evonik Industries (Parsippany, NJ), Fluorine doped Tin Oxide glass (FTO glass) (Pilkington Glass TEC 15 with sheet resistance 15 Ω cm^{-2}) was supplied by Pilkington NA, N3-dye was supplied by Organica® Feinchemie GmbH Wolfen and Surlyn spacer was supplied by Solaronix. All other chemicals used were of reagent grade or better and were supplied by Sigma Aldrich Canada, unless stated otherwise.

Catalyst preparation

Titanium dioxide was obtained following a method modified from that of Kim *et al*.[38] Briefly, 2M $TiOCl_2$ aqueous stock solution was made by the slow addition of ice to $TiCl_4$ chilled to -20°C. TiO_2-PO_4 was precipitated following the addition of distilled water to obtain a concentration of 400 mM to which 45wt% PA was added (33, 56, 78, 111 and 167 µL, corresponding to Ti:PA molar ratios of 146, 88, 63, 44 and 29 respectively) and maintained at 40°C for 24hrs. This reaction was also carried out in the presence of ultrasound using a Branson ultrasonic bath (40 kHz) and the temperature of the water was also maintained at 40°C. Following precipitation the reaction product was centrifuged at 13500 rpm for 20min, washed three times and heat-treated at 600°C for 1 hour.

Photoelectrode fabrication

The electrolyte solution was prepared by mixing two solutions: a titania "suspension" and a "charging" solution [39]. TiO_2-PO_4 precipitate or P25 (2.5 g) were mixed with an ethanol solution (150 mL) containing a small amount of acetylacetone (2.4 mL L^{-1}). The mixture was stirred at room temperature for 5 days in a closed vessel. To this, the charging solution, containing iodine (10 mg), acetone (2.6 mL), water (1.3 mL) and ethanol (100 mL) was added. The electrolyte solution was mixed for 2 hours and sonicated (15-20 minutes) prior to the EPD in order to homogenize the mixture. Fluorine tin oxide (FTO) glass substrates were cleaned with ethanol, mild soap, thoroughly rinsed with deionized water (18.2 MΩ) and dried in a filtered air stream.

The electrophoretic cell contained two FTO glass electrodes, one anode and one cathode serving as a working and counter electrode respectively. These electrodes were placed vertically in a glass beaker (80 mL) with a linear distance between the two electrodes of 20 mm. The cathodic EPD process was carried out at a constant voltage of 5V vs. Ag/AgCl and a time varying between 60 to 500 seconds at room temperature. Subsequently, the coated substrates were rinsed with deionized water, dried in air at room temperature (25°C) and finally sintered at 600°C in air for 1 h. The deposition area was about 5.0 cm^2. The mass of deposited material was calculated from the weight gain of the FTO glass after EPD and sintering at 600°C. The TiO_2-PO_4 films were sensitized with N3-dye by immersing warm (80–100°C after sintering) photo-electrodes in an ethanolic dye solution in ethanol (0.5 mM) and storing them overnight at room temperature. The dye-covered electrodes were then rinsed with ethanol and left to dry in air. A sandwich-type cell was assembled to measure the *i*–V curves using a platinized FTO glass as a counter-electrode. A 50 mm surlyn spacer was positioned between the two electrodes. The composition of the electrolyte was 0.6 M dimethylpropylimidazolium iodide, 0.1 M LiI, 0.05 M I_2, 0.5 M tert-butylpyridine in acetonitrile. For comparison, electrodes prepared from commercial P25 were also used to prepare DSSCs by the same method.

Characterisation procedures

Transmission electron micrographs and electron diffraction patterns were recorded using a Philips CM200 HR-TEM operating at an accelerating voltage of 200 kV. Lattice space measurements of the digital micrographs were made by taking the average of at least 10 lattice spacings using Image tool v3.00. SEM analysis was performed using Hitachi S-4700 FEG-SEM operating at an accelerating voltage of 5 kV (Hitachi, Tokyo, Japan). X-ray diffraction analysis was performed with Cu Ka X-rays with a Bruker X-ray diffractometer (Model D8) across a 2q range of 10-80°. The diffraction spectra were processed using DIFFRACplus Eva (Version 7) software with reference to Powder Diffraction File database (PDF 4+ 2008) of the International Center for Diffraction Data (Newton Square, PA). The crystalline size was calculated from X-ray line broadening using Scherrer's equation:

$$D = 0.9\, l/b \cos q, \qquad \text{Equation 2}$$

where D is the crystal size, l the wavelength of X-ray radiation (0.15418nm for Cu Ka radiation), b is the full width at half maximum (FWHM) and q is the diffraction angle. The mass fraction of anatase was determined from the relative diffraction intensities of anatase [101] (I_A) and rutile [110] (I_R) peaks according to the following Equation 2[40]:

$$\text{Anatase \%} = [0.79I_A / (I_R + 0.79I_A)] \times 100 \qquad \text{Equation 3}$$

Specific surface area measurements were made using the Brunauer-Emmet-Teller (BET) method (Tristar 3000, Micromeritics, Norcross, GA). Samples were degassed under vacuum for 12 hours at 25 °C prior to analysis. Zeta potential measurements to determine isoelectric points were made using a Malvern Zetasizer Nano ZS dynamic light scattering instrument (Malvern Instruments, Worcestershire, UK). Samples were suspended at a concentration of approximately 10 mg L^{-1} in 1 mM aqueous $NaNO_3$ adjusted to various pH values using NaOH and HNO_3. Measurements were also made in the electrophoretic deposition solution of pH 2.94. The electrophoretic mobility of pure rutile and pure anatase were measured using the same instrument. Diffuse reflectance spectra were recorded using a Varian Cary 5000 spectrophotometer fitted with a Praying Mantis diffuse reflectance attachment. The incident beam was collimated and the reflected light captured by an integrating sphere. Electrochemical measurements were performed using a PARSTAT 2273 (Princeton Applied Research). Photo-electrochemical characterizations of the photo-electrodes were performed in 0.1M potassium-phosphate buffer at pH= 7.0 with and without ultraviolet (UV) light. UV illumination was provided by a 100W long wave (365 nm) high intensity UV spot lamp (Blak-Ray, Ted Pella, Reading CA). Photovoltaic measurements were performed using a PG-STAT30 potentiostat (Autolab) and solar simulator at AM1.5 G, where the light intensity was adjusted with an NREL calibrated Si solar cell with a KG-5 filter to 1 sun intensity (100 mW cm^{-2}). In this work more than one cell was prepared; standard errors were calculated for these conditions.

Conclusions

The concept of using a buffering or optically scattering layer that simultaneously reduced recombination rate in a bilayer single compound system was recently reported using spray pyrolysis of two layers of zinc oxide differing in density[32]. In this work, we tailored the electrophoretic deposition of a phase mixture to create a similarly advantageous hierarchical nanostructured films in a single step. This simple and straightforward procedure to prepare composite electrodes with tailored properties could quite easily be scaled up for industrial purposes.

Acknowledgements

The authors gratefully acknowledge the support of the Natural Sciences and Engineering Research Council of Canada. The authors gratefully acknowledge the support of Organica® Feinchemie and NSG / Pilkington NA for the donation of N3-dye and FTO glass, respectively.

Notes and references

[a] Faculty of Dentistry, McGill University, Montreal, H3A 2B2, (Canada).
[b] Department of Mining and Materials Engineering, McGill University, Montreal, H3A 0C5, (Canada)
[c] Department of Surgery, Montreal General Hospital, Faculty of Medicine, McGill University, Montreal, (Canada)

Electronic Supplementary Information (ESI) available: Supplementary methods providing additional details on the materials specification and determination of diffuse reflectance spectra, current-voltage curves of the dye-sensitized solar cells as well the solar cell parameters. See DOI: 10.1039/b000000x/

[1] B. Oregan, M. Gratzel, Nature 1991, 353, 737.
[2] K. Tanaka, M. F. V. Capule, T. Hisanaga, Chemical Physics Letters 1991, 187, 73.
[3] G. Riegel, J. R. Bolton, Journal of Physical Chemistry 1995, 99, 4215.
[4] D. C. Hurum, A. G. Agrios, K. A. Gray, T. Rajh, M. C. Thurnauer, The Journal of Physical Chemistry B 2003, 107, 4545.
[5] T. Kawahara, Y. Konishi, H. Tada, N. Tohge, J. Nishii, S. Ito, Angewandte Chemie-International Edition 2002, 41, 2811.
[6] X. Zhang, Y. Lin, D. He, J. Zhang, Z. Fan, T. Xie, Chemical Physics Letters 2011, 504, 71.
[7] T. Ohno, K. Sarukawa, K. Tokieda, M. Matsumura, Journal of Catalysis 2001, 203, 82.
[8] G. Li, C. P. Richter, R. L. Milot, L. Cai, C. A. Schmuttenmaer, R. H. Crabtree, G. W. Brudvig, V. S. Batista, Dalton Transactions 2009, 10078.
[9] M. Pelaez, N. T. Nolan, S. C. Pillai, M. K. Seery, P. Falaras, A. G. Kontos, P. S. M. Dunlop, J. W. J. Hamilton, J. A. Byrne, K. O'Shea, M. H. Entezari, D. D. Dionysiou, Applied Catalysis B: Environmental 2012, 125, 331.
[10]T. Kawahara, T. Ozawa, M. Iwasaki, H. Tada, S. Ito, Journal of Colloid and Interface Science 2003, 267, 377.
[11]R. Scotti, I. R. Bellobono, C. Canevali, C. Cannas, M. Catti, M. D'Arienzo, A. Musinu, S. Polizzi, M. Sommariva, A. Testino, F. Morazzoni, Chemistry of Materials 2008, 20, 4051; M. Estruga, C. Domingo, X. Domenech, J. A. Ayllon, Nanotechnology 2009, 20; T. K. Yun, S. S. Park, D. Kim, J.-H. Shim, J. Y. Bae, S. Huh, Y. S. Won, Dalton Transactions 2012, 41, 1284.
[12]M. M. R. Jae-Joon Lee, Subrata Sarker, N.C. Deb Nath, A.J. Saleh Ahammad and Jae Kwan Lee, *Metal Oxides and Their Composites for the Photoelectrode of Dye Sensitized Solar Cells, Advances in Composite Materials for Medicine and Nanotechnology*, InTech, 2011.
[13]R. Hattori, H. Goto, Thin Solid Films 2007, 515, 8045.
[14]M. F. Hossain, S. Biswas, T. Takahashi, Thin Solid Films 2008, 517, 1294.
[15]H. Yu, S. Zhang, H. Zhao, G. Will, P. Liu, Electrochimica Acta 2009, 54, 1319.
[16]J. N. Hart, D. Menzies, Y. B. Cheng, G. P. Simon, L. Spiccia, Comptes Rendus Chimie 2006, 9, 622.
[17]Z. Liu, X. Zhang, S. Nishimoto, M. Jin, D. A. Tryk, T. Murakami, A. Fujishima, Langmuir 2007, 23, 10916; Z. Liu, X. Zhang, S. Nishimoto, M. Jin, D. A. Tryk, T. Murakami, A. Fujishima, Langmuir 2007, 23, 10916.
[18]H. Zhang, J. F. Banfield, The Journal of Physical Chemistry B 2000, 104, 3481; D. C. Bassett, Vol. Ph.D., McGill University (Canada), Canada 2011, 263; M. S. Lee, S. S. Park, G.-D. Lee, C.-S. Ju, S.-S. Hong, Catalysis Today 2005, 101, 283.
[19]N. Satoh, T. Nakashima, Y. Kimihisa, in *Sci. Rep.*, Vol. 3 (Ed: N. P. Group), 2013.
[20]U. Gesenhues, Chemical Engineering & Technology 2001, 24, 685.
[21]Z. Yanqing, S. Erwei, C. Zhizhan, L. Wenjun, H. Xingfang, Journal of Materials Chemistry 2001, 11, 1547.
[22]G.-W. Lee, S.-Y. Bang, C. Lee, W.-M. Kim, D. Kim, K. Kim, N.-G. Park, Current Applied Physics 2009, 9, 900; S. Nakade, Y. Saito, W. Kubo, T. Kitamura, Y. Wada, S. Yanagida, The Journal of Physical Chemistry B 2003, 107, 8607.
[23]F. Cesano, D. Pellerej, D. Scarano, G. Ricchiardi, A. Zecchina, Journal of Photochemistry and Photobiology A: Chemistry 2012, 242, 51.
[24]K. R. Reyes-Gil, E. A. Reyes-García, D. Raftery, Journal of The Electrochemical Society 2006, 153, A1296; V. H. Nguyen, B. H. Nguyen, Advances in Natural Sciences: Nanoscience and Nanotechnology 2012, 3, 023001.
[25]S. Y. Treschev, P. W. Chou, Y. H. Tseng, J. B. Wang, E. V. Perevedentseva, C. L. Cheng, Applied Catalysis B-Environmental 2008, 79, 8.
[26]L. Kőrösi, I. Dékány, Colloids and Surfaces A: Physicochemical and Engineering Aspects 2006, 280, 146.
[27]R. Asahi, T. Morikawa, T. Ohwaki, K. Aoki, Y. Taga, Science 2001, 293, 269.
[28]J. B. Varley, A. Janotti, C. G. Van de Walle, Advanced Materials 2011, 23, 2343.
[29]M. F. Hossain, S. Biswas, T. Takahashi, Thin Solid Films 2008, 517, 1294; R. Hattori, H. Goto, Thin Solid Films 2007, 515, 8045.
[30]U. Holzwarth, N. Gibson, Nature nanotechnology 2011, 6, 534.
[31]K. Suttiponparnit, J. Jiang, M. Sahu, S. Suvachittanont, T. Charinpanitkul, P. Biswas, Nanoscale Res Lett 2011, 6, 27.
[32]Y. Y. Peralta-Ruiz, E. M. Lizcano-Beltrán, D. Laverde, P. Acevedo-Peña, E. M. Córdoba, Química Nova 2012, 35, 499.
[33]A. Zaban, M. Greenshtein, J. Bisquert, ChemPhysChem 2003, 4, 859.
[34]H. Yang, W. Fan, A. Vaneski, A. S. Susha, W. Y. Teoh, A. L. Rogach, Advanced Functional Materials 2012, 22, 2821.
[35]C.-H. Lee, W.-H. Chiu, K.-M. Lee, W.-F. Hsieh, J.-M. Wu, Journal of Materials Chemistry 2011, 21, 5114.
[36]J.-M. Kim, S.-W. Rhee, Electrochimica Acta 2012, 83, 264.

[37]G. Veerappan, K. Bojan, S.-W. Rhee, Renewable Energy 2012, 41, 383.
[38]H. D. Nam, B. H. Lee, S. J. Kim, C. H. Jung, J. H. Lee, S. Park, Japanese Journal of Applied Physics Part 1-Regular Papers Short Notes & Review Papers 1998, 37, 4603.
[39]A. Zaban, O. Micic, B. Gregg, A. Nozik, Vol. 14, 1998.
[40]U. Holzwarth, N. Gibson, Nature Nanotechnology 2011, 6, 534.

Table of contents

The plant derived chelating agent phytic acid was found to promote aqueous formation of anatase. By then electrodepositing in an organic solvent the biphasic rutile-anatase mixture could be separated to form a graded heterojunction. A time series characterisation confirmed that a large increase in photocurrent density (0.4 to 0.75 mA/cm^2) coincided with the appearance of anatase in the coating. In a DSSC a 188% higher short current density and 24% higher conversion efficiency using the nanostructured electrodes compared with P25 controls.